Total and partial cross sections for electron capture in collisions of hydrogen atoms with fully stripped ions

R. K. Janev,[*] D. S. Belić,[†] and B. H. Bransden[‡]

Joint Institute for Laboratory Astrophysics, University of Colorado and National Bureau of Standards, Boulder, Colorado 80309

Systematic investigations of charge-transfer reactions $H(1s) + A^{Z+} \rightarrow H^+ + A^{(Z-1)+}(n,l)$ (A^{Z+} being a fully stripped ion) within the multichannel Landau-Zener theory with rotational coupling included (MLZRC) are presented. Total cross-section (σ) calculations in the energy region 0.03—80 keV/amu for selected projectiles with charges $5 \leq Z \leq 74$ are performed. Oscillations in the Z dependence of σ are observed at low collision energies in the low-Z region. Above this region the Z dependence of σ is linear. The n,l distributions of captured electrons are investigated and results for the partial cross sections σ_n for a number of reactions are presented. The maxima of n distributions appear at $n_m \approx Z^{3/4}$ (in accordance with other theoretical predictions) and have a weak velocity dependence. Validity and limitations of the MLZRC model and the obtained results are discussed.

I. INTRODUCTION

The studies of ionization equilibrium, power losses, and neutral-beam heating of magnetically confined plasmas require knowledge of total and partial cross sections for electron-capture reactions between atomic hydrogen and highly stripped ions:

$$H(1s) + A^{Z+} \rightarrow H^+ + A^{(Z-1)+}(n,l) , \qquad (1)$$
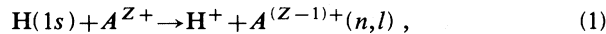
where Z is the ionic charge and n,l are the principal and angular momentum quantum numbers, respectively. The range of ionic species of interest to fusion research is rather wide (extending up to W^{74+}) as is the corresponding collision energy range ($10^{-3} \lesssim E \lesssim 10^3$ keV/amu). Although recent experimental and theoretical work on charge-exchange processes involving multiply charged ions has been very extensive (for the most recent review of this work see Refs. 1—3), systematic investigations of the properties of reaction (1) in a broad range of collision parameters are fairly rare. For the hydrogen atom—fully stripped ion system, which is the most tractable one for the theory, systematic calculations of the total (σ) and partial (σ_n, σ_{nl}) cross sections have been performed by the classical trajectory Monte Carlo (CTMC) method[4—6] and the unitarized distorted-wave approximation (UDWA).[7—9] The energy and charge regions covered by the CTMC investigations are $30 \lesssim E \lesssim 300$ kev/amu and $1 \leq Z \leq 36$, while the UDWA studies are done for $1 \lesssim E \lesssim 500$ kev/amu and $1 \leq Z \leq 20$. Despite their numerical character, these calculations have provided insight in the general properties of total and partial electron-capture cross sections and served as check of some general results obtained using simple analytical models of the process (such as the absorbing sphere model[10] and the electron tunneling theory[11]).

The purpose of this study is to provide a systematic investigation of the charge-exchange reaction (1), with A^{Z+} being a fully stripped ion, by using the multichannel Landau-Zener theory.[12] Our study will be restricted to the energy range $10^{-2} \lesssim E \lesssim 10^2$ kev/amu and ionic charges

$5 \leq Z \leq 74$, and represents a considerable extension of the CTMC and UDWA systematic investigations towards the regions of low E and high Z. With respect to the standard Landau-Zener model, we shall also include in our treatment the effects of rotational coupling between the degenerate Stark states in the ionic channels.[13] The cross-section calculations will be performed specifically for those ions which are at present of primary interest for the controlled thermonuclear fusion research. Atomic units ($\hbar = e = m_e = 1$) will be used throughout this paper, unless otherwise explicitly indicated.

II. METHOD OF CROSS-SECTION CALCULATIONS

The hydrogen atom—fully stripped, high-Z ion system is characterized by a large number of potential-energy curve-crossings (adiabatic pseudocrossings), approximately given by[14]

$$r_0 = \text{Ent}\{(X-1)[X+1-(1+2X)^{1/2}]\}, \quad X = Z^{1/2} \qquad (2)$$

where $\text{Ent}(y)$ is the entire part of y. Owing to the high intrinsic symmetry of the one-electron two-Coulomb center system considered, only one of the n^2 Stark states associated with a given final channel n of reaction (1) interacts with the state in the initial channel, namely, the one whose parabolic quantum numbers are $n_1 = 0$, $n_2 = n-1$, and $m = 0$. The internuclear distance at which this interaction primarily takes place is given by (the diabatic curve-crossing distance)

$$R_n = \frac{n^2(Z-1)}{Z^2-n^2}\left[1 + \left[1 - \frac{3n(n-1)(Z^2-n^2)}{n^2 Z(Z-1)^2}\right]^{1/2}\right], \qquad (3a)$$

$$R_n \simeq \frac{2n^2(Z-1)}{Z^2-n^2}, \quad n < Z \qquad (3b)$$

where in Eq. (3a) the linear Stark effect is accounted for. The interaction between the above-mentioned states gives rise to a splitting $\Delta(R)$ of the corresponding adiabatic energies. By solving numerically the two-Coulomb center eigenvalue problem for the system (H, A^{Z+}) with $4 \leq Z \leq 54$, Olson and Salop[10] obtained the following analytical fit to the energy splittings $\Delta(R_n)$ (within an accuracy of 17%):

$$\Delta(R_n) = 18.26 Z^{1/2} \exp(-1.324 Z^{-1/2} R_n) \ . \tag{4}$$

The quantity $\Delta(R)$, also called exchange interaction, is a measure of the strength of radial coupling between the corresponding states in the pseudocrossing region, giving rise to nonadiabatic transitions in a zone $\delta R_n \simeq \Delta(R_n)/\Delta F_n = R_n^2 \Delta(R_n)/(Z-1)$ around R_n. The characteristic length of variation of the exchange interaction is $l_0 \approx Z^{1/2}/1.324$.

The transitions in a pseudocrossing region may be described by the Landau-Zener model if both the statical width δR_n and the dynamical width $\delta s = 2(v/\Delta F_n)^{1/2} \simeq 2[v R_n^2(Z-1)]^{1/2}$ of the transition zone are much smaller than l_0 (see, e.g., Ref. 15),

$$\delta R_n \ll l_0, \quad \delta s \ll l_0 \ , \tag{5}$$

where v is the relative collision velocity. For typical n values of $n \simeq Z^{3/4}$, which correspond to the mostly populated final states in reaction (1) at low and intermediate energies,[2,6,9] $R_n \sim Z^{1/2}$, $\delta s \sim O(v)$, and the conditions (5) are satisfied provided $v \ll Z$ and Z is sufficiently large. More refined conditions for the applicability of Landau-Zener model for description of collision dynamics in a single pseudocrossing region in reaction (1) are given elsewhere.[13]

The application of the multiple—curve-crossing Landau-Zener theory[12] to the present problem also requires that the distance $\Delta R_{n,n+1}$ between two consecutive diabatic crossings be considerably larger than δR_n. Since for large Z and n,

$$\Delta R_{n,n+1} \simeq 2(Z-1)(2n+1)/(Z^2-n^2) \simeq 2R_n/n \ , $$

it can be easily verified that for $n \simeq Z^{3/4}$, the ratio $(\delta R_n/\Delta R_{n,n+1}) \sim Z^{-1/4}$.

Another point which deserves attention is the question of how the effects of the turning point will influence the applicability region of the Landau-Zener model in the case of reaction (1). As is well known, these effects can be neglected if the following condition is fulfilled[15]:

$$\Phi_0(R_n, R_{t1}, R_{t2}) \gg \xi = \frac{\pi \Delta^2(R_n)}{4v \Delta F_n}, \quad \Delta F_n \simeq \frac{(Z-1)}{R_n^2} \tag{6}$$

where Φ_0 is the difference of adiabatic phases between the crossing point R_n and the turning points R_{t1} and R_{t2}, corresponding to the final-channel potentials $V_n(R)$ and $V_{n+1}(R)$. For the system under consideration and for impact parameters considerably smaller than R_n, $\Phi_0 \sim \Delta R_{n,n+1}$. In this case and for the typical value $n \simeq Z^{3/4}$, the ratio Φ_0/ξ behaves as $\mu v^2 Z^{3/4}$ (μ being the reduced mass of the system), i.e., the condition (6) is more easily satisfied when Z is large. Of course, for impact pa-

rameters close to R_n, the effects of turning point on collision dynamics are strong and the Landau-Zener model becomes inapplicable. Transitions in the system $H + Z^{Z+}$ under such conditions have been considered recently[16] within a model representation of the interaction potentials. The limitations imposed by the condition (6) on the accuracy of the obtained results will be discussed in Sec. IV, together with some other restrictions of the multichannel Landau-Zener method. With this in mind and in view of the above discussion one can represent the transition probability at a single curve-crossing region by the Landau-Zener formula

$$p_n = \exp\left[-\frac{\pi \Delta^2(R)}{2v_R \Delta F(R)}\right]_{R=R_n}, \tag{7}$$

where $v_R = v(1 - b^2/R^2)^{1/2}$ is the radial velocity and b is the impact parameter. (We assume a rectilinear trajectory for the nuclear motion.)

Besides the Landau-Zener—type transitions in the curve-crossing region δR_n, transitions may occur in the (H, A^{Z+}) collision system due to rotation of the internuclear axis. These transitions take place in the region $R < R_n$ when the system is in the ionic state $H^+ + A^{(Z-1)}(n)$ between the populated (by the radial coupling in δR_n) $n_2 = n-1$, $n_1 = m = 0$ parabolic state and the other $n^2 - 1$ unoccupied Stark states. If the collision velocity is not too small, the rotational transitions between the Stark states in the region $R < R_n$ may be considered independently from the Landau-Zener transitions in the δR_n region.[13] The probability for rotational decay of the $n_2 = n-1$, $n_1 = m = 0$ state to all other $n^2 - 1$ Stark states between the first and second passage of the crossing point R_n is given by[13]

$$q_n = 1 - (1 - \sin^2\beta \sin^2\alpha)^{2(n-1)} \ , \tag{8}$$

$$\beta = \arctan\left[\frac{2Zbv}{3n}\right], \tag{9}$$

$$\alpha = \frac{\Delta \chi}{2}\left[1 + \left[\frac{3n}{2Zbv}\right]^2\right]^{1/2}, $$

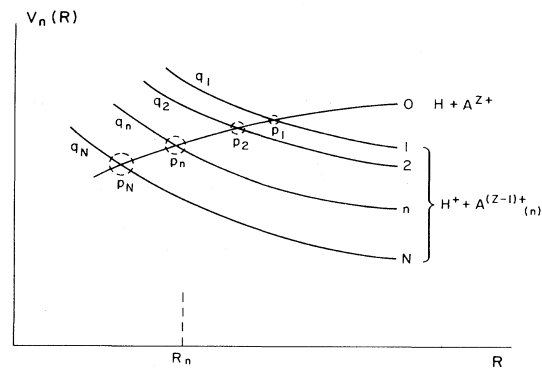and $\Delta \chi$ is the angle of rotation of the internuclear axis,

FIG. 1. Schematic diagram of the potential-energy curves of the system $(H + A^{Z+})$ at large internuclear distances.

$$\frac{\Delta \chi}{2} = \arccos \, (b/R_n) \, . \tag{10}$$

Let us now consider the case when during the collision the initial state interacts strongly with N final product states. Let the ordering of the states be as shown in Fig. 1. Assuming that there are no interferences between the transitions (p_k, p_{k+1}) and (p_k, q_k), the probability that after the collision a particular ionic level n will be populated is given by

$$P_n = p_1 p_2 \cdots p_n (1-p_n)[1+(p_{n+1} p_{n+2} \cdots p_N)^2 + (p_{n+1} p_{n+2} \cdots p_{N-1})^2 (1-p_N)^2 (1-q_N)$$

$$+ (p_{n+1} p_{n+2} \cdots p_{N-2})^2 (1-p_{N-1})^2 (1-q_{N-1}) + \cdots$$

$$+ p_{n+1}^2 (1-p_{n+2})^2 (1-q_{n+2}) + (1-p_{n+1})^2 (1-q_{n+1})]$$

$$+ p_1 p_2 \cdots p_{n-1} (1-p_n)^2 q_n \, . \tag{11}$$

By setting $q_k = 0$ ($k = 1, \ldots, N$) in Eq. (11), one obtains the result of the multichannel Landau-Zener theory.[12]

The partial (σ_n) and total (σ) cross sections of reaction Eq. (1) are respectively given by

$$\sigma_n = 2\pi \int_0^{R_n} P_n b \, db \, , \tag{12}$$

$$\sigma = \sum_{n=1}^{N} \sigma_n \, . \tag{13}$$

Owing to the sharp dependence of p_k on $\Delta(R_k)$, the number of curve-crossing regions contributing considerably to P_n is rather limited. The distance crossings are passed by the system diabatically, whereas the ones with small R_k [and therefore large $\Delta(R_n)$] are avoided adiabatically. The condition $v_R > 0$ also leads to a reduction of the terms in P_n when integrated over the impact parameters. With respect to the usual Landau-Zener model, the effect of inclusion of rotational coupling is a shift of the cross-section maximum towards lower energies and an increase in the value of the cross section in the energy region below the maximum.[13] The inclusion of the influence of the turning point leads to the same effects.[16]

In order to test the above-described multichannel Landau-Zener method with rotational coupling included (MLZRC), we have performed cross-section calculations for the reactions $H + C^{6+} \rightarrow H^+ + C^{5+}$ and $H + O^{8+} \rightarrow H^+ + O^{7+}$, for which accurate large basis (33 states) molecular-orbital close-coupling (MOCC) calculations in a wide energy region exists,[17,18] with a proper account for the electron-momentum-transfer effects. The number of ionic channels included in our calculations was $N = 5$ for the $H + C^{6+}$ case, and $N = 6$ for the $H + O^{8+}$ case. The results of the calculations are shown in Figs. 2 and 3 (the solid curves). They are compared with the results of MOCC calculations of Green and associates[17,18] (open squares) and Salop and Olson[19,20] (dot-dashed curves), and with those of UDWA[8,7] (dashed curves). The experimental points in Fig. 6 are for C^{6+} (open circles, Ref. 21) and
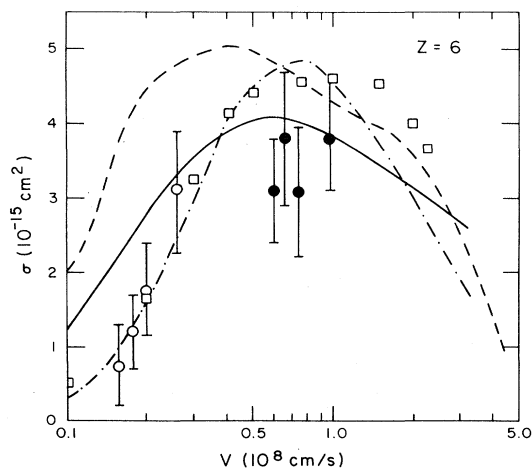

FIG. 2. Total cross sections for the $H + C^{6+} \rightarrow H^+ + C^{5+}$ reaction. Solid curve, present calculations; dashed curve, UDWA theory (Ref. 8); dot-dashed curve, six-state MOCC calculations (Ref. 19); open squares, 33-state MOCC calculations (Ref. 17). Experimental data: open circles are for $H + C^{6+}$ (Ref. 21) and closed circles are for the $H + O^{6+}$ system (Ref. 22).

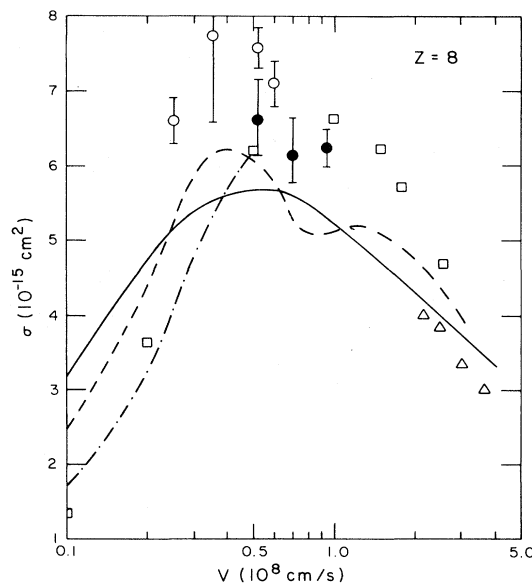FIG. 3. Total cross sections for the $H + O^{8+} \rightarrow H^+ + O^{7+}$ reaction. Solid curve, present calculations; dashed curve, UDWA theory (Ref. 7); dot-dashed curve, eight-state MOCC calculations (Ref. 20); open squares, 33-state MOCC calculations (Ref. 18); triangles, CTMC results (Ref. 20). Experimental points are for Xe^{8+} (open circles) and Ar^{8+} (closed circles) from Ref. 23.

for O^{6+} (closed circles, Ref. 22) and in Fig. 3 for Xe^{8+} (open circles) and Ar^{8+} (closed circles) taken from Ref. 23. The agreement of MLZRC results for $H + C^{6+}$ with the 33-state MOCC calculations of Green et al.[17] is within 50% except in the lowest part of the velocity region considered. The situation for the $H + O^{8+}$ case is similar. The open triangles in Fig. 3 are the results of the CTMC method.[20] As can be seen from these two examples, in the velocity region below the cross-section maximum, the MLZRC method tends to overestimate the cross-section values, and this tendency seems to increase with increasing Z. This effect, absent in the MLZ model without inclusion of rotational coupling, is most probably connected with the fact that the assumption about the degeneracy of all the n^2 Stark states in the region $R \leq R_n$ breaks down when R_n is small (i.e., for the lower values of n). Namely, in this case the state $n_2 = n - 1$, $n_1 = m = 0$ may significantly be decoupled from the other $n^2 - 1$ Stark states and its rotational decay onto them may be much smaller than that given by Eq. (8). The last term in Eq. (11) then gives a spurious contribution to the population probability P_n.

Despite the recognized limitations of the MLZRC method, it is still useful to undertake a systematic investigation of the total and partial cross sections of reaction (1), since the use of more accurate methods (like a large basis MOCC) for high Z is associated with enormous computational efforts. On the other side, the information provided by the systematic cross-section studies within the MLZRC model will give an insight into the character of approximations involved in other generalized treatments of reaction (1) (such as the decay models).

III. RESULTS OF THE CALCULATIONS

Using the method described in Sec. II, we have performed total and partial cross-section calculations for reaction (1) with A^{Z+} being a completely stripped ion having charge between $Z = 5$ and 74. For ions with $Z \leq 36$, all reaction channels have been included in the calculations, i.e., $N = Z - 1$. For ions with $Z > 36$, the number of channels was taken to be $N = 35$, which, except for the case of W^{74+}, provides convergence of the results within 1%. The calculations have been performed in the energy region from 3×10^{-2} to 70 keV/amu. Below 3×10^{-2} kev/amu the inaccuracy of the data is expected to be about a factor of 2, or even larger for $Z \geq 20$. For $E \geq 70$ keV/amu, the MLZRC model also becomes unreliable due to the neglected electron-momentum-transfer effects. Note, however, that for Eq. (1), the adiabatic condition is $v \lesssim Z^{1/4}$ and for $Z \geq 10$ it is well satisfied in the whole energy region considered.

A. Total cross sections

Apart of the total charge-exchange cross sections for the $H + C^{6+}$ and $H + O^{8+}$ systems, discussed in Sec. II, we have calculated the total cross sections of Eq. (1) for the following fully stripped ions: N^{7+}, F^{9+}, Ne^{10+}, Al^{13+}, Si^{14+}, Cl^{17+}, Ar^{18+}, Ca^{20+}, Ti^{22+}, Cr^{24+}, Fe^{26+}, Ni^{28+}, Cu^{29+}, Kr^{36+}, Zr^{40+}, Mo^{42+}, Cd^{48+}, Xe^{54+}, and W^{74+}. The results of the calculations are shown in Figs.
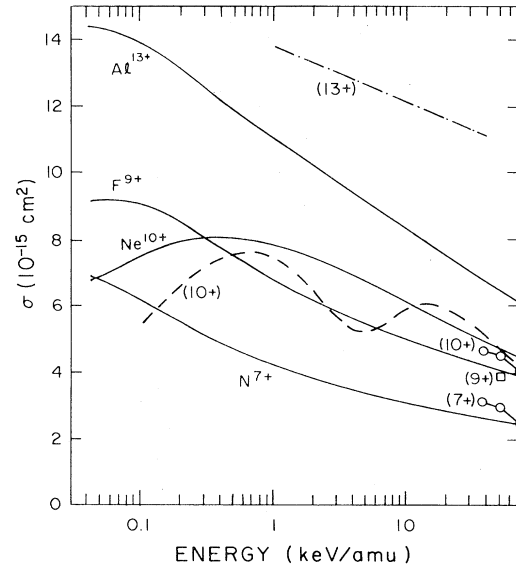

FIG. 4. Total cross sections for the fully stripped ions N^{7+}, F^{9+}, Ne^{10+}, and Al^{13+} in atomic hydrogen. Solid curves are the results of present calculations. Symbols are results for the CTMC calculations: open circles are for N^{7+} and Ne^{10+} (Ref. 4) and the square is for F^{9+} (Ref. 6). Dashed curve for Ne^{10+} is the UDWA result (Ref. 9) and the dot-dashed curve for Al^{13+} is the DM result (Ref. 24).
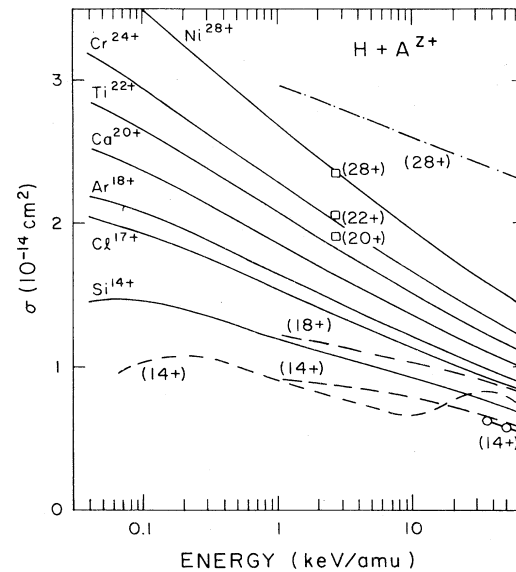

FIG. 5. Total charge-exchange cross sections of Si^{14+}, Cl^{17+}, Ar^{18+}, Ca^{20+}, Ti^{22+}, Cr^{24+}, and Ni^{28+} in atomic hydrogen. Solid curves are results of the present calculations. Open circles for Si^{14+} are the CTMC results (Ref. 6), the short- and long-dashed curves are, respectively, the UDWA (Ref. 9) and the classical (analytical) model result (Ref. 25) for the same ion. Long-dashed curve for Ar^{18+} and the dot-dashed curve for Ni^{28+} are, respectively, the classical (Ref. 25) and the decay (Ref. 24) model results. Squares for Ca^{20+}, Ti^{22+}, and Ni^{28+} are the ASM results (Ref. 10).
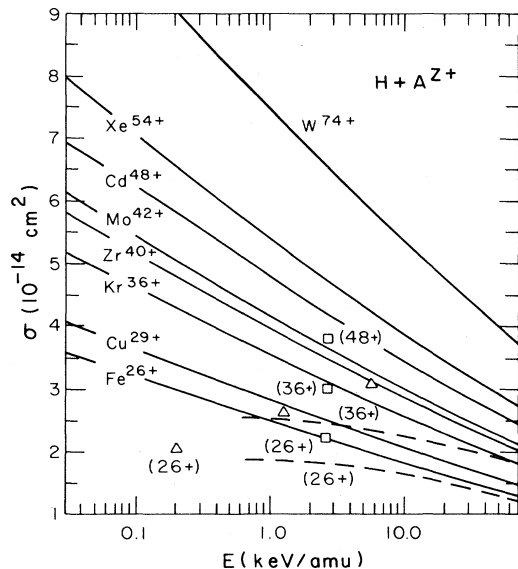
FIG. 6. Total charge cross sections of Fe^{26+}, Cu^{29+}, Kr^{36+}, Zr^{40+}, Mo^{42+}, Cd^{48+}, Xe^{54+}, and W^{74+} in atomic hydrogen. Solid curves are the results of present calculations. Dashed curves are the classical model results (Ref. 25) for Fe^{26+} and Kr^{36+}. Open triangles are the 17-state MOCC results for Fe^{26+} (Ref. 26). Squares are the ASM results (Ref. 10).

4—6 (the solid curves). The MLZRC cross section for $H + N^{7+}$, $H + F^{9+}$, and $H + Ne^{10+}$ (see Fig. 4) in the high-energy region are compared with the results of CTMC calculations of Olson and Salop[4] (for N^{7+} and Ne^{10+}, open circles) and Olson[6] (for F^{9+}, the open square). For the case of $H + Ne^{10+}$ comparison is also made with the results of the UDWA[9] (the dashed line). We would like to note that the UDWA results in the region below ~ 1 keV/amu are also not reliable. Our cross section for the $H + Al^{13+}$ system (see Fig. 4) is compared with the results obtained in the decay model (DM) of Duman and Smirnov[24] (the dot-dashed curve). Owing to the neglected back capture and the assumption of a continuous spectrum of ionic levels to which an electron can be captured, the DM significantly overestimates the charge-exchange cross section. In the considered energy range the DM gives an upper bound of the charge-exchange cross section.

In Fig. 5 the total cross sections for the $H + Si^{14+}$, Cl^{17+}, Ar^{18+}, Ca^{20+}, Ti^{22+}, Cr^{24+}, and Ni^{28+} colliding systems are presented. The cross section for $H + Si^{14+}$ is compared with the CTMC results[4] (the open circles), the UDWA results[9] (short-dashed curve), and the analytic classical model[25] (long-dashed line). Comparison with the classical model calculations[25] is also made for the $H + Ar^{18+}$ colliding system. It is worthwhile to note that this model takes into account only the electron-capture transitions from the region $b \leq R_c = 2(2Z-1)^{1/2}$ and neglects the under-barrier electron capture from the $b > R_c$ region. The contribution of the under-barrier (Landau-Zener—type) transitions to the cross section at low energies is, however, quite significant. The dot-dashed line in Fig. 5 is the DM result[24] for $H + Ni^{28+}$, lying again con-

siderably higher than the present data. The open squares for $Z = 20$, 22, and 28 are the results of the absorbing sphere model (ASM).[10]

The total charge-exchange cross section for Fe^{26+}, Cu^{29+}, Kr^{36+}, Zr^{40+}, Mo^{42+}, Cd^{48+}, Xe^{54+}, and W^{74+} are shown in Fig. 6. The cross sections for Fe^{26+} and Kr^{36+} in the region above 0.5 keV/amu are compared with the results of the analytical classical model,[25] which lie below MLZRC values. The open squares for Fe^{26+}, Kr^{36}, and Cd^{48+} are the ASM results[10] and they are consistent with our data. The three open triangles for Fe^{26+} are results of the 17-state MOCC calculations.[26] The discrepancy between the MLZRC and MOCC results, particularly at the energy of 0.2 keV/amu (about 50%) is quite significant.

The fact that for $Z > 36$ we have included only $N = 35$ exit channels in our calculations did not affect the cross-section results for $Z \leq 54$. In the case of W^{74+} we used a plausible extrapolation of the values of σ_n from the region $n \leq 35$ into the region $n > 35$. Since in the considered region the maximum of the n distributions for W^{74+} lies around $n_m \approx 28$, the contribution of the partial cross sections σ_n with $n > 35$ is only a few percent of the total cross section. Thus, the employed extrapolation procedure does not include an uncertainty in the cross sections presented in Fig. 6 higher than $\sim 3-5\%$. We should also point out that Eq. (4) for $\Delta(R_n)$ has been derived only for $4 \leq Z \leq 54$. However, its extrapolation to the case of W^{74+} seems to be plausible.

Another question may be raised in connection with the high values of nuclear charges involved in our calculations: the role of relativistic effects. Keeping in mind that in the considered energy region the electron capture dominantly populates those ionic states which are energetically resonant with the initial state, it is clear that no relativistic effects can be expected to influence the total charge-exchange cross section. In this energy region the low-lying ionic states are populated with an extremely small probability, so that for all practical purposes no relativistic effects have to be taken into consideration in the calculations.

The total cross sections for all the reactions considered here have a slow, logarithmic dependence on the collision
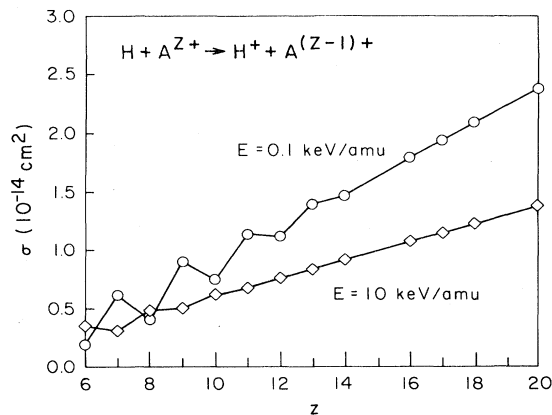

FIG. 7. Z dependence of the total charge-exchange cross sections at collision energies of 0.1 and 10 keV/amu.

velocity in the region above the cross-section maximum. The following analytical fit to all of the calculated cross sections can be derived (where σ is in cm^2):

$$\sigma = 2.25 \times 10^{-16} Z \ln \left[\frac{15}{v} \right] ,$$

$$0.04 \leq v \leq 1.8, \quad Z \geq 16 . \quad (14)$$

In the considered velocity and ionic charge regions, the above analytical formula represents the calculated data within a 5% accuracy. The inaccuracy of Eq. (14) increases rapidly when Z decreases due to the appearance of the cross-section maxima for some of the ions in the lower part of the considered velocity domain (see Figs. 4 and 5 for examples).

For a given collision velocity, the total cross section σ as a function of Z has a linear behavior down to some $Z_c = Z_c(v)$, such that for $Z < Z_c(v)$, $\sigma(Z)$ begins to oscillate. This is illustrated in Fig. 7 for two collision energies: $E = 0.1$ and 10 kev/amu. The figure shows that with increasing the collision energy, the value of Z_c decreases. The amplitude of Z oscillations increases with decreasing the collision energy. The origin of low-energy Z oscillations in the total charge-transfer cross sections is the discreteness of projectile ion energy spectrum and the resonant selectivity of the process at a given energy. Maxima in $\sigma(Z)$ occur when (for a given energy) there is only one final level n_m on which the electron capture dominantly takes place. If for a given Z there is no such an
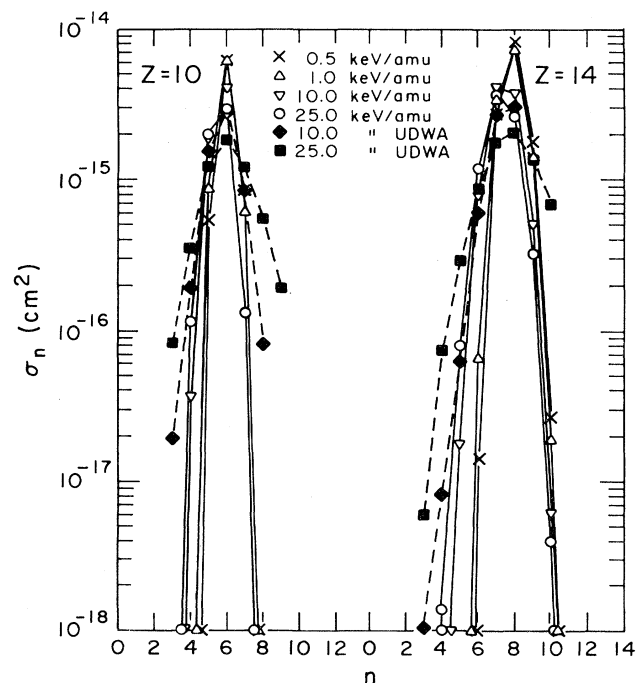
adjacent (resonant) level, a minimum appears in the cross section $\sigma(Z)$. As will be seen in Sec. III B, the resonant selectivity is expressed more at low energies and low Z. For high Z and E, a larger number of final states is quasiresonantly coupled with the initial one and the selec-

FIG. 9. n distributions of captured electrons in Eq. (1) for different Z values and at $E = 0.5$ keV/amu.

FIG. 8. n distributions of captured electrons in H + Ne^{10+} →H$^+$ + Ne$^{9+}(n)$ and H + Si^{14+}→H$^+$ + Si$^{13+}(n)$ reactions for $E = 0.5$, 1, 10, and 25 keV/amu. Symbols connected by solid lines are the results of present calculations. Symbols connected by dashed lines are the results of UDWA calculations (Ref. 9).
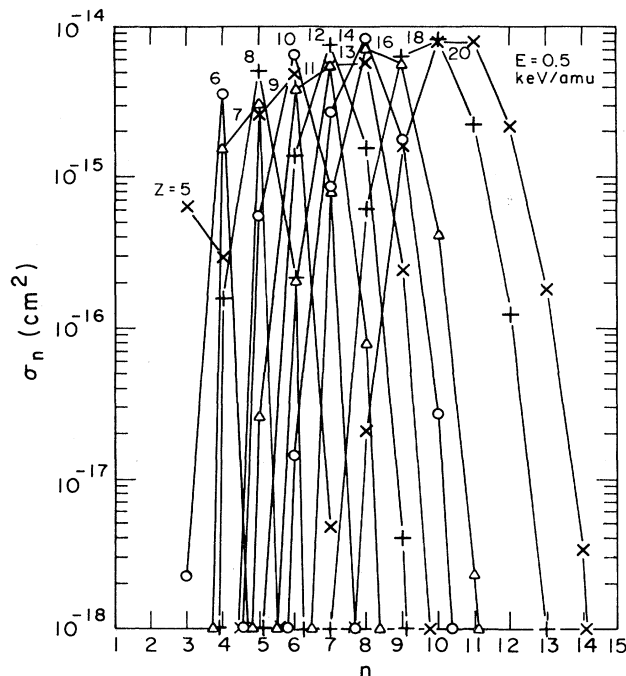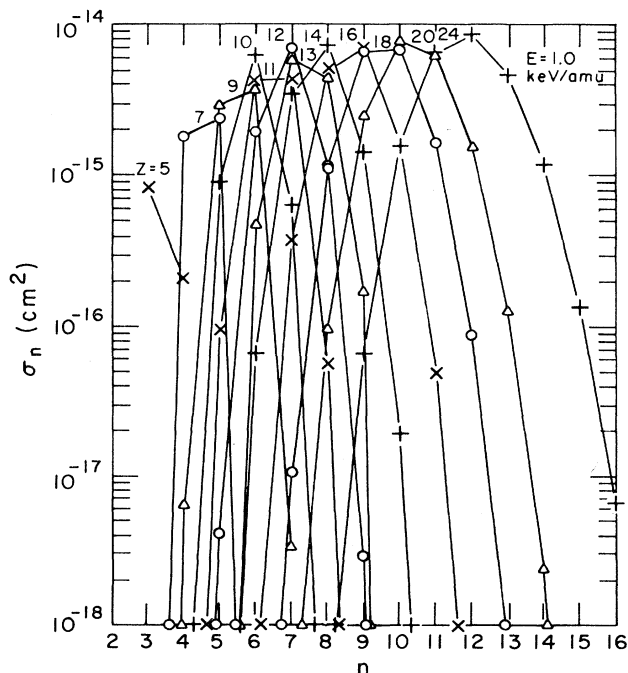

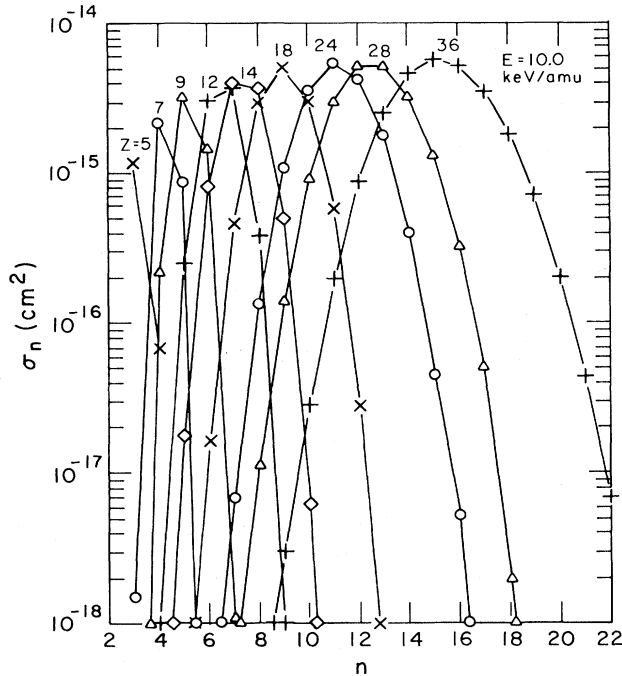FIG. 10. n distributions of captured electrons in Eq. (1) for different Z values and at $E = 1$ keV/amu.

FIG. 11. n distributions of captured electrons in Eq. (1) for different Z values and at $E = 10$ keV/amu.

tivity of the process is weakened. This leads to smearing out of the Z oscillations. Let us mention that low-energy Z oscillations in the total electron-capture cross sections have also been predicted by other models,[16,27,28] and that they have also been experimentally observed.[29−31]
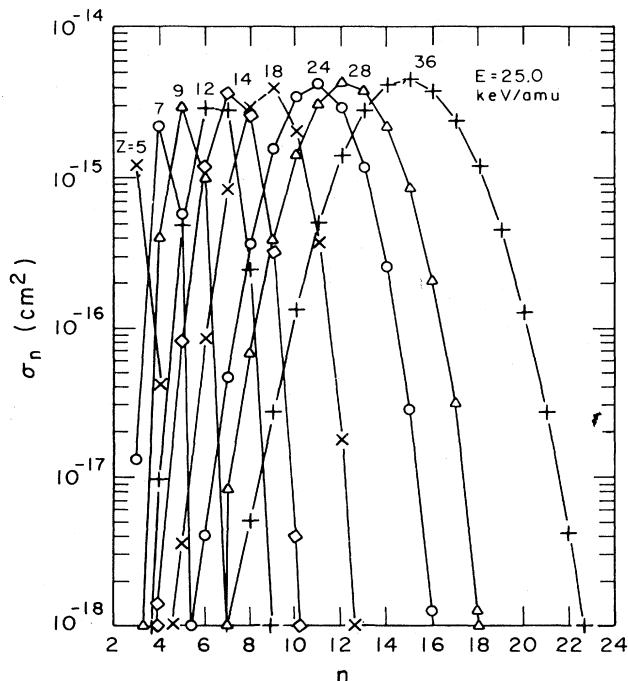

FIG. 12. n distributions of captured electrons in Eq. (1) for different Z values and at $E = 25$ keV/amu.

B. Partial cross sections

In connection with the population of specific final states in Eq. (1) two aspects are important: the distributions of captured electrons over the final-state quantum numbers n and l and the velocity dependence of the partial cross sections σ_n and σ_{nl}. We have investigated these questions within the MLZRC model for the range of Z and E considered here.

Let us consider first the n distributions. In Fig. 8 we present the n distributions for the $H + Ne^{10+}$ and $H + Si^{14+}$ colliding systems at four collision energies: $E = 0.5$, 1, 10, and 25 keV/amu. For these reactions the distributions are peaked at $n_m = 6$ (for Ne^{10+}) and $n_m = 8$ (for Si^{14+}), and decrease rapidly when $|n - n_m|$ increases. For $E = 10$ and 25 keV/amu, comparison is made with the UDWA n distributions.[9] Significant discrepancy between the MLZRC and UDWA results can be observed at the wings of the distributions.

A systematic presentation of the n distributions obtained within the MLZRC model is given in Figs. 9—12 for $E = 0.5$ keV/amu ($5 \leq Z \leq 20$), 1 keV/amu ($5 \leq Z \leq 24$), 10 keV/amu ($5 \leq Z \leq 34$), and 25 keV/amu ($5 \leq Z \leq 36$). With increasing Z, the number of open channels in Eq. (1) increases and an increasingly larger number of product states are significantly populated. Consequently, the width of the distributions becomes larger for higher Z. For a given energy, the energy distributions have maxima at $n_m \approx Z^{0.768}$, in accordance with the UDWA results.[9] At the energies of $E = 0.5$ and 1 kev/amu, the maxima of n distributions are peaked at the even values of Z (except for $Z = 5$), while for odd Z values two values of n, in the neighborhood of $Z^{0.768}$, share the electron capture. This gives rise to oscillations in the Z dependence of the total cross section (see Fig. 7). With increasing the energy and Z, this situation changes. For $E = 10$ and 25 keV/amu, the n distributions for the odd-Z ions are sharply peaked at one value of n. It can also be noticed from Figs. 8—12 that for a given Z, n_m slightly decreases with increasing energy. This is more explicitly demonstrated in Fig. 13, where the velocity dependence of different σ_n for the
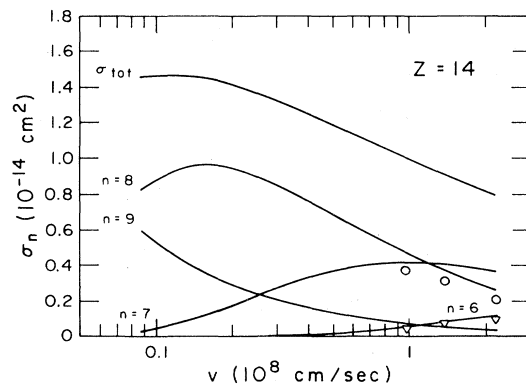

FIG. 13. Velocity dependence of partial cross sections σ_n for the reaction $H + Si^{14+} \rightarrow H^+ + Si^{13+}(n)$. Solid lines, results of present calculations. Symbols, UDWA results (Ref. 13) for $n = 8$ (open circles) and $n = 6$ (inverted triangles).
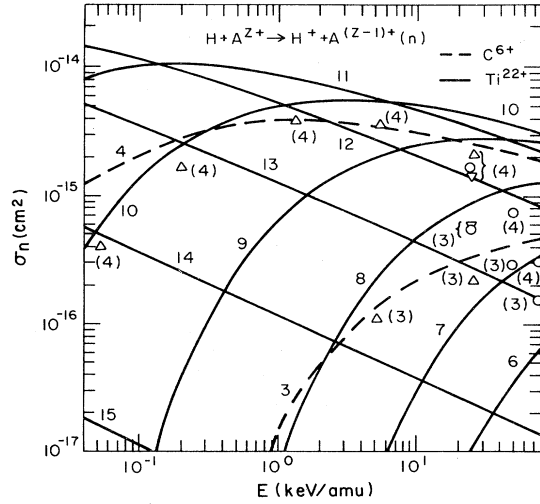
FIG. 14. Partial cross sections for capture into a particular principal shell n in H + C^{6+}, Ti^{22+} collisions. Dashed curves are for C^{6+} and the solid curves are for Ti^{22+}. All other points (n) are results for C^{6+} obtained by other methods: open triangle, 33-state MOCC calculations (Ref. 17); inverted triangle UDWA results (Ref. 9); open circle, CTMC results (Ref. 6).

FIG. 16. Same as for Fig. 14, except a for Ne^{10+} ions: triangles are the UDWA results (Ref. 9); closed and open circles are the CTMC results of Refs. 5 and 6, respectively.

H + Si^{14+} case is shown. It can be seen from this figure that only in the velocity region from 6×10^6 to 1.2×10^8 cm/sec the level $n=8$, as predicted by the UDWA expression $n_m \simeq Z^{0.768}$, is dominantly populated, whereas below and above this region the levels $n=9$ and 7 become, respectively, dominantly populated.

A systematic presentation of the energy dependence of partial cross sections σ_n for $Z=6$, 8, 10, 13, 22, 24, 26, and 28 is given in Figs. 14—17. The results for σ_n of mostly populated levels in the $Z=6$, 8, 10 cases are com-

pared with the data from UDWA, CTMC, and MOCC calculations. Reasonable agreement between the MLZRC results and the results of other methods is found only for the dominantly populated levels n_m in a given collision energy region. With increasing $|n - n_m|$, the discrepancy becomes increasingly larger. The reason for this is that the MLZRC cannot account for transitions into levels with $n \geq Z$ [see Eq. (3)] and for levels n approaching $n_{max} = (Z - 1)$ the method becomes less and less appropriate to describe collision dynamics. On the other hand, for n smaller than n_m, the present model overestimates σ_n due to the spuriously large contribution of the last term in Eq. (11), as discussed in Sec. II.

Let us now discuss briefly the distributions of captured electrons over the quantum numbers l of a given n. Within the MLZRC model this problem was discussed by
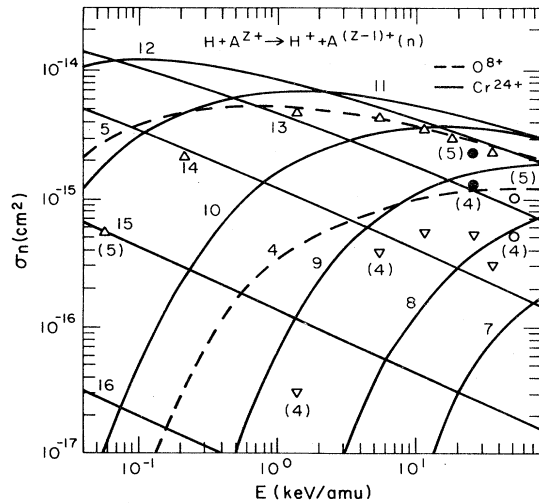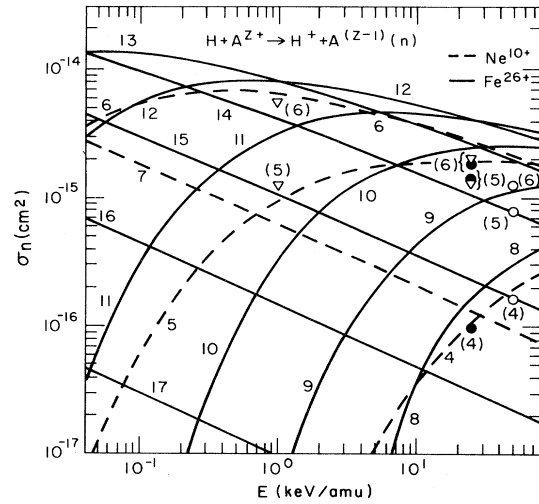

FIG. 15. Same as for Fig. 14, except for O^{8+} (dashed curves) and Cr^{24+} (solid curves). Closed and open points are CTMC results for O^{8+} from Refs. 5 and 6, respectively. Symbols $\triangle$ and ∇ refer, respectively to the $n=5$ and 4 results of 33-state MOCC calculations (Ref. 18).
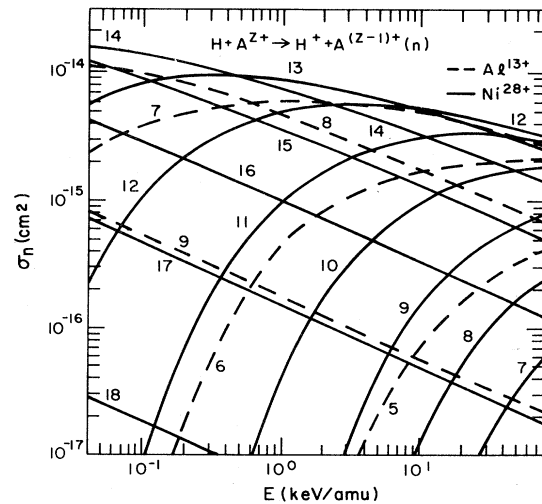

FIG. 17. Same as for Fig. 14, except for Al^{13+} (dashed curves) and Ni^{28+} (solid curves).

Abramov et al.[32] The rotational coupling is proportional to the angular velocity $\omega_n = vb/R_n^2 \sim v/R_n$, where R_n is the crossing distance. For very small values of ω_n, the Stark state $n_2 = n - 1$, $n_1 = m = 0$, populated by the radial coupling at the first pass of transition region δR_n, can be considered as being little depopulated by rotation of the internuclear axis. By going from the parabolic into an angular momentum representation of this state, one immediately obtains the l distribution of captured electrons[32]

$$W_{nl} = (2l+1)\frac{[(n-1)!]^2}{(n+l)!(n-1-l)!} \ . \tag{15}$$

In the opposite case of large ω_n, the rotational mixing of Stark states is strong and one should expect a statistical distribution of l sublevels,

$$W_{nl}^{st} = (2l+1)/n^2 \ . \tag{16}$$

Equation (15) predicts a maximum of W_{nl} at $l = 1$ for $n \leq 8$ which shifts towards higher values of l with increasing n. For very high n Eq. (15) can be represented in the form[16]

$$W_{nl} \simeq \frac{(2l+1)}{n}\exp\left[-\frac{l(l+1)}{n}\right] \tag{17}$$

with a maximum at $l_m \lesssim n^{1/2}$. In contrast to Eqs. (15) and (17), Eq. (16) predicts that in the strong mixing regime the maximum of the l distributions is at $l_m = n - 1$. With respect to the region of applicability of the above equations for W_{nl}, we would like to point out the following. Since R_n depends both on n and Z, the angular mixing parameter ω_n depends on three parameters: v, n, and Z. Thus, for given v and Z, both mixing regimes can be met by varying n. Equations (15) and (16) are obtained under the assumption that the mixing takes place only in the region $R \leq R_n$ where rotational coupling is pronounced. However, mixing of angular momentum states may also take place in the region $R > R_n$ due to the long-range interactions between the products.

IV. CONCLUDING REMARKS

In this paper we have performed a systematic investigation of the total and partial cross sections for electron-capture reaction in the low-energy collisions between hydrogen atoms and fully stripped ions. We have used a multichannel Landau-Zener model with allowance for the rotational transitions between the Stark states in the final channels. Those ions from the charge state region $5 \leq Z \leq 74$ are selected which are of primary interest to current controlled fusion research. The energy region investigated extends from 3×10^{-2} to 80 keV/amu. The main failures of the employed MLZRC method are the neglect of (a) the transition to product states with $n \geq Z$; (b) breakdown of the degeneracy of the $n_2 = n - 1$, $n_1 = m = 0$ state with the other $n^2 - 1$ Stark states in the region $R < R_n$, when R_n is small; (c) the effects of turning point R_{tn} when it becomes close to the crossing point R_n; and (d) the electron-momentum-transfer effects, which become important at the upper edge of the energy range considered. We note that the last two failures are common to all versions of the Landau-Zener model, whereas the first two are specific for the MLZRC model. Points (a), (b), and (c) affect the accuracy of the cross section in the lower energy region (below ~ 0.1 keV/amu), particularly when Z increases. Their combined effect may lead to a significant overestimation of the cross section in this region, which for $Z \gtrsim 30$ may reach a factor of 2 or so. In the region $E \gtrsim 70$ keV/amu, particularly for lower-Z ions, the neglected electron-momentum-transfer effects lead also to an overestimation of the cross section by the MLZRC model. In the region $0.1 \lesssim E \lesssim 70$ keV/amu, the MLZRC model provides results for the toal electron-capture cross sections which for high Z are consistent with the absorbing sphere model and have an accuracy of about $\pm 50\%$. However, it should be noted that the velocity dependence of σ for high Z, even in this region, is somewhat steeper than the one predicted by the classical model[25] or suggested by the MOCC calculations for $Z = 26$.[26]

The partial cross sections σ_n, calculated with the MLZRC model, have an accuracy of about $\pm 50\%$ in a more restricted region of energy than for the total cross section, and only for those n which are dominantly populated. For $n < n_m$ the method usually overestimates σ_n, while for $n > n_m$ it underestimates σ_n. These errors mutually cancel in the total cross section, thus extending the energy range in which its accuracy is reasonable. We also note that the 17% uncertainty of Eq. (14) for $\Delta(R)$ may also introduce an uncertainty of about $\pm 40\%$ in the calculated partial and total cross sections.

---

*On leave of absence from the Institute of Physics, Belgrade, Yugoslavia.

†On leave of absence from the Faculty of Natural Sciences, Belgrade University, Belgrade, Yugoslavia.

‡On leave of absence from the University of Durham, Durham DH1 3HP, Great Britain.

[1]H. B. Gilbody, Phys. Scr. **23**, 143 (1981); **24**, 712 (1981).
[2]R. K. Janev and L. P. Presnyakov, Phys. Rep. **70**, 1 (1981).
[3]P. T. Greenland, Phys. Rep. **81**, 131 (1982).
[4]R. E. Olson and A. Salop, Phys. Rev. A **16**, 531 (1977).

[5]A. Salop, J. Phys. B $\underline{12}$, 919 (1979).

[6]R. E. Olson, Phys. Rev. A $\underline{24}$, 1726 (1981).

[7]H. Ryufuku and T. Watanabe, Phys. Rev. A $\underline{18}$, 2005 (1978).

[8]H. Ryufuku and T. Watanabe, Phys. Rev. A $\underline{19}$, 1538 (1979).

[9]H. Ryufuku and T. Watanabe, Phys. Rev. A $\underline{20}$, 1828 (1979).

[10]R. E. Olson and A. Salop, Phys. Rev. A $\underline{14}$, 576 (1976).

[11]T. P. Grozdanov and R. K. Janev, Phys. Rev. A $\underline{17}$, 880 (1978).

[12]S. S. Gershtein, Zh. Eksp. Teor. Fiz. $\underline{43}$, 706 (1962) [Sov. Phys.—JETP $\underline{43}$, 501 1963)]; A. Salop and R. E. Olson, Phys. Rev. A $\underline{13}$, 1312 (1976).

[13]V. A. Abramov, F. F. Baryshnikov, and V. S. Lisitsa, Zh. Eksp. Teor. Fiz. $\underline{74}$, 897 (1978) [Sov. Phys.—JETP $\underline{47}$, 469 (1979)].

[14]L. I. Ponomarev, Zh. Eksp. Teor. Fiz. $\underline{55}$, 1836 (1968) [Sov. Phys.—JETP $\underline{28}$, 971 (1969)].

[15]E. E. Nikitin and S. Ya. Umanskii, *Nonadiabatic Transitions in Slow Atomic Collisions* (Atomizdat, Moscow, 1979) (in Russian).

[16]L. P. Presnyakov, D. B. Uskov and R. K. Janev, Zh. Eksp. Teor. Fiz. $\underline{83}$, 933 (1982) [Sov. Phys.—JETP $\underline{83}$, 525 (1982)].

[17]T. A. Green, E. J. Shipsey, and J. C. Browne, Phys. Rev. A $\underline{25}$, 1364 (1982).

[18]E. J. Shipsey, T. A. Green, and J. C. Browne, Phys. Rev. A $\underline{27}$, 821 (1983).

[19]A. Salop and R. E. Olson, Phys. Rev. A $\underline{16}$, 1811 (1977).

[20]A. Salop and R. E. Olson, Phys. Rev. A $\underline{19}$, 1921 (1979).

[21]R. A. Phaneuf, I. Alvarez, F. W. Meyer, and D. H. Crandall, Phys. Rev. A $\underline{26}$, 1892 (1982).

[22]D. H. Crandall, R. A. Phaneuf, and F. W. Meyer, Phys. Rev. A $\underline{19}$, 504 (1979).

[23]D. H. Crandall, R. A. Phaneuf, and F. W. Meyer, Phys. Rev. A $\underline{22}$, 379 (1980).

[24]E. L. Duman and B. M. Smirnov, Fiz. Plazmy $\underline{4}$, 1161 (1978) [Sov. J. Plasma Phys. $\underline{4}$, 650 (1978)].

[25]T. P. Grozdanov, J. Phys. B $\underline{13}$, 3835 (1980).

[26]A. Salop and R. E. Olson, Phys. Lett. $\underline{71A}$, 407 (1979).

[27]H. Ryufuku, K. Sasaki, and T. Watanabe, Phys. Rev. A $\underline{21}$, 745 (1980).

[28]L. P. Presnyakov, D. B. Uskov, and R. K. Janev, Phys. Lett. $\underline{84A}$, 243 (1981).

[29]V. V. Afrosimov, A. A. Basalaev, E. D. Donets, and M. N. Panov, Pis'ma Zh. Eksp. Teor. Fiz. $\underline{31}$, 635 (1980) [JETP Lett. $\underline{31}$, 600 (1981)].

[30]H. Schrey and B. A. Huber, J. Phys. B $\underline{14}$, 3197 (1981).

[31]T. Iwai, Y. Kaneko, M. Kimura, N. Kobayashi, S. Ohtani, K. Okuno, S. Takagi, H. Tawara, and S. Tsurubuchi, Phys. Rev. A $\underline{26}$, 105 (1982).

[32]V. A. Abramov, F. F. Baryshnikov, and V. S. Lisitsa, Zh. Eksp. Teor. Fiz. Pis'ma Red. $\underline{27}$, 494 (1978) [JETP Lett. $\underline{27}$, 464 (1978)].